UC Irvine
UC Irvine Previously Published Works

Title

Simulation study of protoacoustics as a real-time in-line dosimetry tool for FLASH proton therapy

Permalink

Journal

ISSN

Authors

Kim, Kaitlyn

Pandey, Prabodh Kumar

Gonzalez, Gilberto

et al.

Publication Date

DOI

Copyright Information

Peer reviewed

RESEARCH ARTICLE

Simulation study of protoacoustics as a real-time in-line dosimetry tool for FLASH proton therapy

Kaitlyn Kim[1] | Prabodh Kumar Pandey[2] | Gilberto Gonzalez[3] | Yong Chen[3] | Liangzhong Xiang[1,2,4]

[1]Department of Biomedical Engineering, University of California, Irvine, California, USA

[2]Department of Radiological Sciences, University of California, Irvine, California, USA

[3]Department of Radiation Oncology, University of Oklahoma College of Medicine, Oklahoma City, Oklahoma, USA

[4]Beckman Laser Institute & Medical Clinic, University of California, Irvine, California, USA

Correspondence
Liangzhong Xiang, Department of Radiology/BME, University of California, Irvine, CA, USA.
Email: liangzhx@hs.uci.edu

Abstract

Background: Applying ultra-high dose rates to radiation therapy, otherwise known as FLASH, has been shown to be just as effective while sparing more normal tissue compared to conventional radiation therapy. However, there is a need for a dosimeter that is able to detect such high instantaneous dose, particularly in vivo. To fulfill this need, protoacoustics is introduced, which is an in vivo range verification method with submillimeter accuracy.

Purpose: The purpose of this work is to demonstrate the feasibility of using protoacoustics as a method of in vivo real-time monitoring during FLASH proton therapy and investigating the resulting protoacoustic signal when dose per pulse and pulsewidth are varied through multiple simulation studies.

Methods: The dose distribution of a proton pencil beam was calculated through a Monte Carlo toolbox, TOPAS. Next, the k-Wave toolbox in MATLAB was used for performing protoacoustic simulations, where the initial proton dose deposition was inputted to model acoustic propagations, which were also used for reconstructions. Simulations involving the manipulation of the dose per pulse and pulsewidth were performed, and the temporal and spatial resolution for protoacoustic reconstructions were investigated as well. A 3D reconstruction was performed with a multiple beam spot profile to investigate the spatial resolution as well as determine the feasibility of 3D imaging with protoacoustics.

Results: Our results showed consistent linearity in the increasing dose-per-pulse, even up to rates considered for FLASH. The simulations and reconstructions were performed for a range of pulsewidths from 0.1 to 10 μs. The results show the characteristics of the proton beam after convolving the protoacoustic signal with the varying pulsewidths. 3D reconstruction was successfully performed with each beam being distinguishable using an 8 cm $\times$ 8 cm planar array. These simulation results show that measurements using protoacoustics has the potential for in vivo dosimetry in FLASH therapy during patient treatments in real time.

Conclusion: Through this simulation study, the use of protoacoustics in FLASH therapy was verified and explored through observations of varying parameters, such as the dose per pulse and pulsewidth. 2D and 3D reconstructions were also completed. This study shows the significance of using protoacoustics and provides necessary information, which can further be explored in clinical settings.

KEYWORDS
flash proton therapy, in vivo dosimetry, ionoacoustics, protoacoustics

1 | INTRODUCTION

Cancer is a disease that results in the death of over a half million of people globally each year, making it stand as the second leading cause of deaths.[1] One of the major treatment modalities is radiation therapy, which has been developed and clinically applied for nearly a century.[2] However, the toxicity and side effects that occur with prolonged treatment can prove to be detrimental to a patient's health as the surrounding normal tissues around the tumor begin to receive damage as well.[3] In a study by Favaudon et al., applying ultra-high dose rates (also termed FLASH) in radiation therapy resulted in clinical outcomes just as effective as conventional radiation dose rate, but with far less severe damage to the normal tissues, as the treatment delivery time is being decreased to less than a second.[4] Current literature has defined FLASH as dose rates that are greater than 40 Gy/s, which is 400 times greater than conventional radiation therapy dose rates ($\sim$0.01–0.4 Gy/s).[5,6] Such high dose rates are already observed in the clinic, although this is typically done using pencil beam systems (PBS).[7,8] Due to the high tissue sparing, FLASH radiotherapy has gained particular interest in radiobiology studies and current treatment machines are furthering their technology to be able to implement it. A variety of preclinical studies have been performed demonstrating the benefits of FLASH compared to conventional therapy.[9–11]

However, despite the benefits of FLASH, finding a radiation dosimeter capable of detecting such high instantaneous dose or dose rates has proven a difficult task.[12] With FLASH progressively becoming an area that many wish to progress into clinical settings, there is a higher demand for safer and efficient quality assurance methods.[13] Current detectors require the use of correction factors due to the saturation effects that occur due to ultra-high dose rate (UHDR). Therefore, there is a significant need from the scientific community to identify the best solution and approach for UHDR dosimetry.[5,14]

Several dosimeters have been explored for FLASH purposes already.[14–17] Ion chambers (IC) have been incorporated in FLASH studies. However, to account for the high instantaneous dose rates seen in FLASH, a correction factor needs to be applied to correct for ion-recombination to use ICs. Along with saturation and poor temporal resolution ($\sim$ms), ICs do not make to be ideal real-time dosimeters. Chemical dosimeters such as Alanine have been used for FLASH purposes. Dose-rate independence with this dosimeter type is high (3×10^{10} Gy/s).[18] However, doses lower than 2 Gy cannot be measured, and real-time measurements are not possible.[19] Within chemical dosimeters, radiochromic film has also been explored in FLASH settings with success due to its dose-rate independence. However, the measurements cannot be performed in real-time, and

readings are done offline. Several luminescent detectors, such as Thermo-luminescent Dosimeters (TLD) and Fluorescent Nuclear Track Detectors (FNTD) have been used in FLASH studies, both shown to have excellent dose-rate independence and large dynamic ranges.[20,10] However, there is still a lack of real-time readout for these methods as well.

High imaging speed and no saturation at higher dose rates are important for achieving real time, in vivo dosimetry for FLASH during patient treatment. Radiation-induced acoustics is a novel alternative technology that shows promise for in vivo FLASH dosimetry. The use of acoustic signals as a method of monitoring and verification has been studied since 1991 during proton and ion therapy and is shown to be a feasible technique for real-time monitoring.[21–23] This method of using such thermoelastic pressures upon proton irradiation was coined as protoacoustics. Protoacoustics is an in vivo range verification method which measures the proton range based on the time of flight within submillimeter accuracy.[24–29] This is considered to be possible as the dose deposition can be reconstructed using these pressure waves.[30] It provides many benefits over other dosimetry tools because of its improved spatial resolution.[31,32] It is also possible to avoid the problem of saturation, which is a great issue within proton FLASH therapy. Because of its great benefits, protoacoustics is already being used in preclinical studies.[33] Protoacoustics has shown great potential in dosimetry for conventional proton therapy.[27] However, there are limits that remain unclear, such as whether the linearity between protoacoustic signal strength and proton dose holds in the FLASH regime. Additionally, it is important to understand how pulse variation would affect protoacoustic signals in clinical proton machines.

Previous studies involving simulations and measurements on an electron beam with FLASH properties (>40 Gy/s) have been investigated before using a modified linac. The paper from Sunbul et al. investigated the simulation workflow for ionizing radiation acoustic imaging (iRAI).[34] Various characteristics, such as the pulse duration and linearity, were investigated to show the potential iRAI has for in vivo dosimetry in FLASH. Linearity in the FLASH regime for electron therapy has also been demonstrated experimentally.[35] Oraiqat et al. demonstrated dose measurements with the use of a dual ultrasound and iRAI system.[35] However, electron therapy is limited to superficial radiotherapy. In contrast, our research aims to investigate the potential of protoacoustic imaging to monitor proton FLASH therapy for deep-seated tumors in a clinical setting.

To the best of our knowledge, this is the first simulation paper which investigates the parameters and characteristics of protoacoustics under FLASH therapy conditions. The characteristics and guidelines for FLASH are still not well defined, as the main contributing

factors for this phenomenon are not standardized. Thus, we have performed simulations to observe the resulting protoacoustic signal for varied dose per pulse and pulsewidths achieved by current FLASH proton sources and studied the effects of these parameters on the reconstructed single beam dose maps. Within proton therapy, there are also techniques that incorporate the use of multiple small beam spots. Many of these are classified under the concept of spatially fractioned radiation therapy (SFRT).[36] LATTICE radiation therapy (LRT) also falls under SFRT, and has been used in over 150 patients.[37] Because of the growing interest for this area of therapy, we also explore the reconstruction of such a case via protoacoustics.

Protoacoustics has shown great potential in dosimetry for conventional proton therapy.[38] However, there are limits that remain unclear, such as whether the linearity between protoacoustic signal strength and proton dose holds in the FLASH regime. Several proton machines have been modified to produce FLASH by varied dose per pulse and puplsewidth.[39,40] Therefore, characterizing the protoacoustic signal with these different parameters is essential in order to apply them to these clinical proton machines. Additionally, it is important to understand how pulse variation would affect protoacoustic signals, both in clinical proton machines and novel proton sources, such as laser-driven proton sources.

2 | MATERIALS AND METHODS

2.1 | The protoacoustic effect

The initial acoustic pressure (p_0) can be related to the dose deposited (D) through the equation:

$$P_0 = \Gamma\rho D, \tag{1}$$

where Γ represents the Gruneisen coefficient, a dimensionless parameter and ρ is the density for water.

The propagation of the protoacoustic waves can be described by the thermoacoustic wave equation[41]:

$$\nabla^2 p\left(\vec{r}, t\right) - \frac{1}{v_s^2}\frac{\partial^2}{\partial t^2}p\left(\vec{r}, t\right) = -\frac{\beta}{C_p}\frac{\partial}{\partial t}H\left(\vec{r}, t\right), \tag{2}$$

where $H(\vec{r}, t)$ is the heat deposition at point $\vec{r}$ and time t, v_s is the speed of sound in medium, β is the thermal expansion coefficient, and C_p is the specific heat capacity.[42] The pressure wave equation can be simplified by assuming that each individual proton pulse deposits the heat energy instantaneously. Therefore, the protoacoustic measurement will reveal (1) the proton Bragg peak (BP) location during the dose delivery and (2) the dose amount deposited to the target volume,

which can be reconstructed using tomographic reconstruction algorithms. The workflow behind FLASH proton therapy is explained further in Figure 1.

### 2.2 | Acoustic propagation and proton transport simulations

All acoustic propagation simulations were completed using the k-Wave toolbox in MATLAB.[43] K-Wave is a simulation and reconstruction toolbox that can model photoacoustic wave fields. Using k-Wave, the parameters for the initial acoustic pressure were predefined, with $\Gamma = 0.11$ and $\rho = 1000$ kg/m^3, which are measured values in distilled water.[44,45] The proton pencil beam dose distributions were modeled using TOPAS (Toolkit for Particle Simulation) version 3.1.2.[46] TOPAS is a Geant4 simulation extension toolkit which can model X-ray and particle therapy. It can allow the user to edit material composition and beam parameters to obtain proton beam range or stopping power as reported in PSTAR database or NIST tables.[47] The beam spot size was set to sizes from 1.0 to 3.0 mm along with several shifts in X-Y plane position. A water phantom geometry was used for collecting the dose deposition. The water phantom dimensions were 8 cm × 8 cm × 30 cm with a 0.5 mm resolution per voxel. The 3D grid resolution used was 0.5 mm voxels. The simulated dose distribution is obtained as a table file which is sent to MATLAB as input for the k-Wave simulation.

2.3 | Simulation 1. Variation of dose per pulse

The first set of simulations consisted in varying the dose per pulse between 0.2 and 20 cGy/pulse. Pulsewidth was kept constant at 4 μs. The same Gaussian pulse shape was used for convolutions for each of the dose per pulse simulations. All of the simulations performed were in 3D with 0.5 mm resolution using a 200 MeV proton beam simulated in TOPAS. A 5 cm × 5 cm 16 × 16 grid planar array was used as the detector and placed 5 cm past the center of the Bragg peak. To provide more realistic results, noise was added to the signals. This was completed by using the 'awgn' function in MATLAB. The function offers the flexibility to add white noise based on the simulated protoacoustic signal strength, which is proportional to the dose per pulse.

2.4 | Simulation 2. Variation of pulsewidths

The second set of simulations were completed by varying the pulsewidth between 0.1 and 20 μs at a constant dose rate of 5 cGy/pulse. The pulsewidths used for the
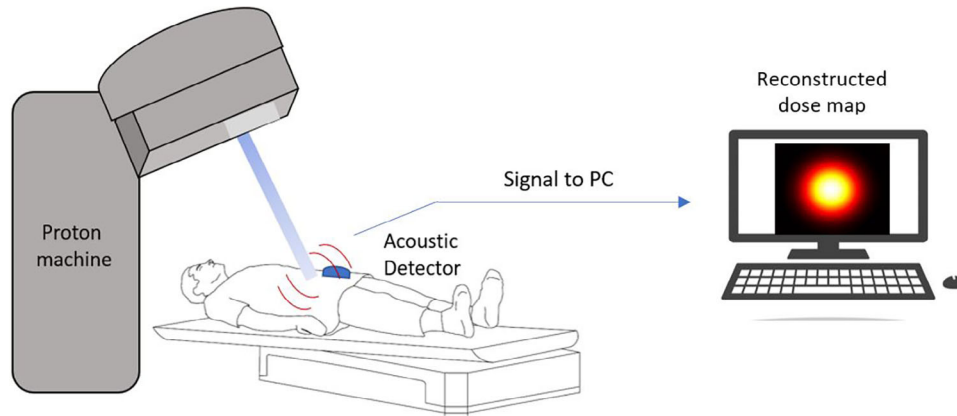
FIGURE 1 Basic workflow of FLASH proton therapy. The clinical pencil beam system irradiates the target with the greatest amount of the energy being deposited at the Bragg peak. This irradiation generates acoustic pressure waves, which are detected and can then undergo image reconstruction to view the dose deposition.

simulations are well within thermal confinement, and were verified using the equation for thermal relaxation time:

$$T_{th} = \frac{d_c{}^2}{4D_T}, \qquad (3)$$

'd_c' is the desired spatial resolution, and 'D_T' is the thermal diffusivity. The value for D_T is $\sim 0.114 \frac{mm^2}{sec}$ for soft tissue, while d_c was around 1 mm, which is the smallest beam size that was used for the simulations.[48]

Similar to Simulation 1, the same dimension planar array was used as the detector and the 200 MeV proton beam was implemented. To vary the pulsewidth, a Gaussian pulse was convoluted with the acoustic pressure signal. The following equation for the Gaussian pulse was used:

$$G(t) = \frac{1}{\sigma\sqrt{2\pi}} \exp\left(-\frac{1}{2}\frac{(t-\mu)^2}{\sigma^2}\right), \qquad (4)$$

where μ refers to the position of the center of the pulse and σ refers to the Gaussian RMS width.

2.5 | Simulation 3. 2D Reconstruction of varied pulsewidths

The third set of simulations included 2D time-reversal reconstructions for each of the varied pulsewidths. A circular sensor with a 3 cm radius and 128 detector points was used and placed concentric to the BP volume and in the BP plane. The layout for this setup is shown in Figure 2(a). The total time for pressure traces was 70.7 μs for the time-reversal reconstruction. The sampling frequency used was 20 MHz, and the number of samples during this time was 1415. The measurement

data were generated at a grid with higher resolution (0.5 mm) and the time-reversal reconstructions were evaluated at a relatively coarser grid (0.4 mm).

## 2.6 | Simulation 4. 3D reconstruction of 9 microbeam profile

A 150 MeV 9 beam spot proton profile (mimicking SFRT) laid out in a 3 by 3 grid was created in TOPAS. Each beam was 1 mm in size with 1 cm separation. A 3D simulation assuming an impulse heating pulse (δ-pulse) and a 3D time-reversal reconstruction were completed for measurements generated at an 8×8 cm (16×16 elements) planar array placed 5 cm behind the BP. The reconstructions were also performed for the measurements corresponding to 1, 2, and 4 μs pulsewidths. To characterize the reconstructions, Gaussian fitting was performed for to obtain each of their full width at half maximum (FWHM) as well as the peak reconstructed doses. The FWHMs of the reconstructed beamlets from the fitted Gaussian RMS widths (σ) were evaluated using:

$$FWHM = 2\sqrt{2\ln(2)}\sigma \qquad (5)$$

3 | RESULTS

3.1 | Results from varied dose simulations

The initial pressure in the k-Wave simulation was changed based on varying doses per pulse to demonstrate the linearity for protoacoustics. Figure 3(a) shows the results of the simulations when the dose is varied from 0.2 to 20 cGy/pulse with the pulsewidth constant at 4 μs. 0.2 cGy/pulse is a range considered to be used in
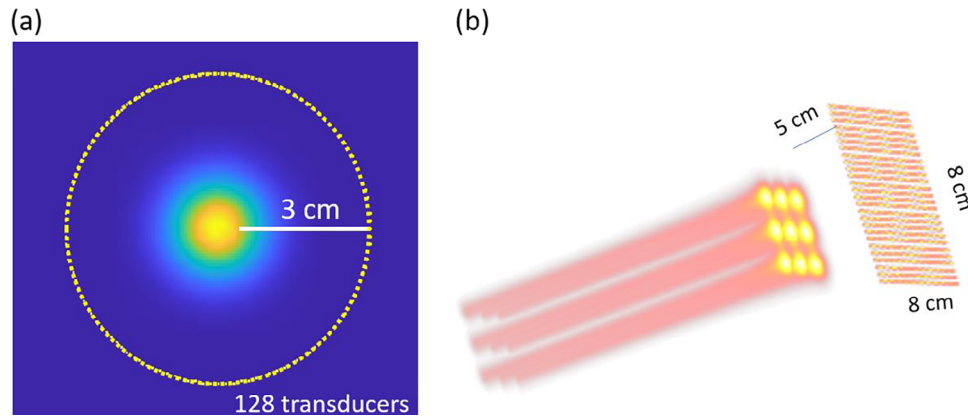
FIGURE 2 Demonstration of the layouts for each simulation in k-Wave. (a) Overview of the circular sensor mask used for the 2D reconstruction and the pressure source overlaid inside. (b) Overview of the planar array used for the 3D reconstruction of the multiple beam spots.
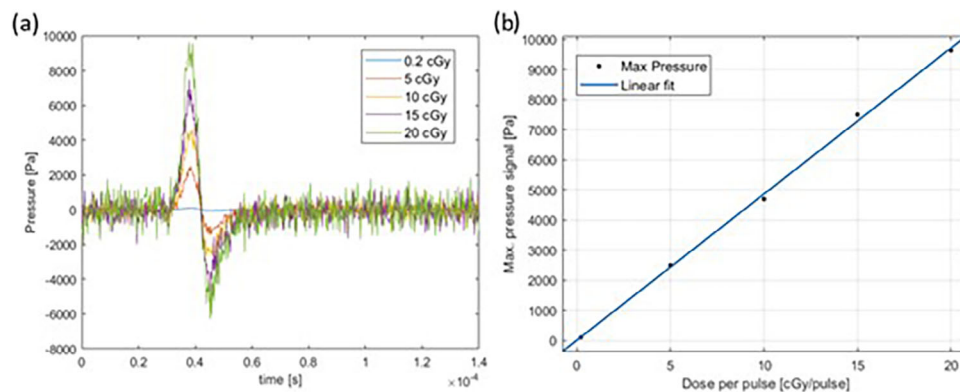
FIGURE 3 (a) Protoacoustic signals simulated using k-Wave toolbox for doses varied between 0.2 and 20 cGy with added white Gaussian noise. (b) Variation of the pressure signal amplitudes with dose per pulse.

conventional radiation therapy, while the rest are within FLASH range.[49] This was done to demonstrate that linearity holds for both conditions. Previous protoacoustic studies have used SNR values between 5 and 30 dB to account for different background noises that may occur.[50] Therefore, white Gaussian noise was added to the signal to obtain 5 dB SNR to provide realistic results. To better show the linearity between the dose and pressure, Figure 3(b). provides a line of best fit across the maximum pressure of each dose from Figure 3(a). The linear fit has an R^2 value of 0.99.

3.2 | Results from varied pulse widths

To vary the pulsewidth of the signal to demonstrate the effects of the pulse duration on the signal, the impulse protoacoustic response was convoluted with the Gaussian pulse shape function. The protoacoustic signal from the center detector was taken, and the maximum value from these signals across the multiple dose per

pulse values were presented in Figure 4. In Figure 4 the results for the simulation for varied pulsewidths is shown. Figure 4(a) shows the protoacoustic signals corresponding to the various pulsewidths between 0.1 and 20 μs while keeping a constant dose of 20 cGy/pulse. To see the trend that occurs with varied pulsewidths, Figure 4(b) plots the maximum of the protoacoustic signals from Figure 4(a) with respect to the corresponding pulsewidths and displays them in the exponential curve fit. The exponential curve is fitted to the pulsewidths larger than 1 μs with an R^2 value of 0.995. Figure 4(c) shows the results from the 2D time-reversal reconstruction that was done for each of the pulsewidths.

3.3 | Results from the 9 beam reconstruction

3D TR reconstructions were performed on the 9 beam spot profile set in a 3 cm × 3 cm grid to determine if
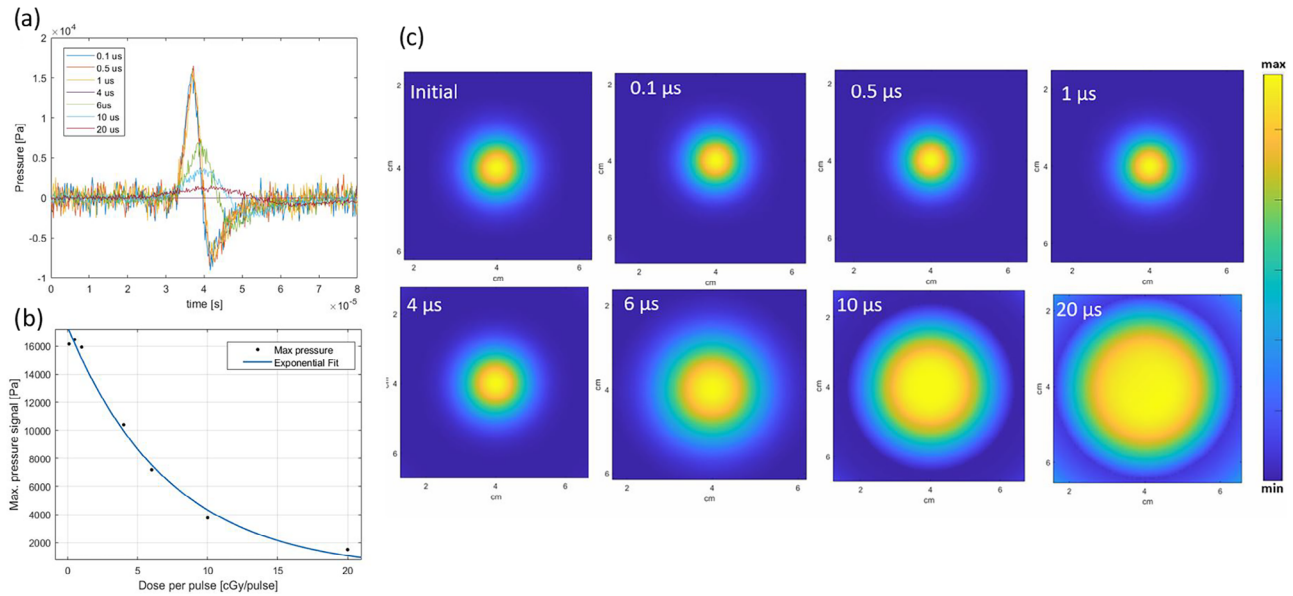
FIGURE 4 (a) Protoacoustic signals simulated from the k-Wave toolbox with varied pulsewidths and consistent dose per pulse. (b) Showing the relationship between signal amplitudes and dose per pulse with an exponential curve fitted with the pulsewidths greater than 1 μs. (c) 2D reconstructions for varied pulsewidths, with "Initial" representing the incident beam to compare with the varied pulsewidths. Increase in beam size is seen with increasing pulsewidths.
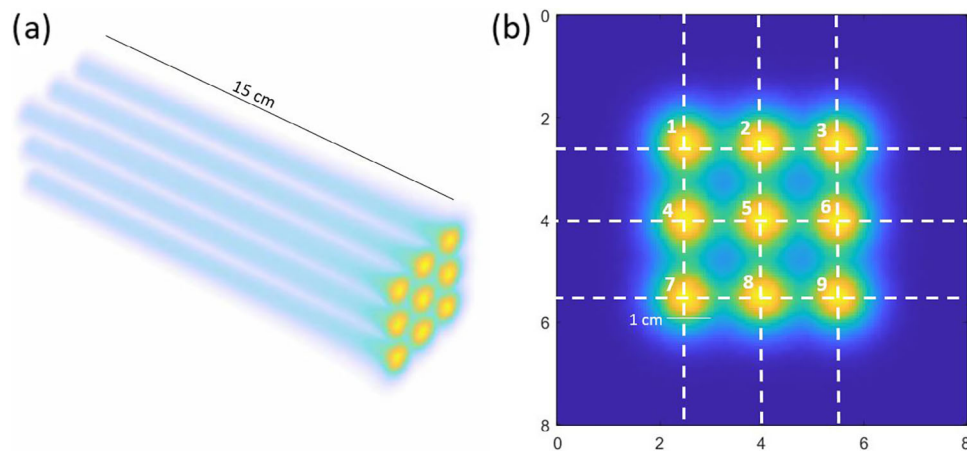
FIGURE 5 (a) Initial dose deposition of the 150 MeV 9 spot beam file with 1 cm beam spot size for each. (b) initial dose deposition with a slice of the XY plane taken directly at the maximum dose of the 9 spot beam profile. The vertical and horizontal dotted lines across the figure represent where the FWHM was taken along.

visualization of individual beamlet was possible using protoacoustic tomographic reconstructions. Figure 5 shows the initial dose profile in a 3D view and as an XY slice. The reconstructed BP plane slice corresponding to δ-pulse excitation is shown in Figure 6(a) and the 3D rendering of the reconstructed dose map is depicted in Figure 6(b). With increasing temporal pulsewidths the width of each reconstructed beamlet increases, as also seen in Figure 4 for the 2D case. The FWHMs for the beamlets at the BP plane along with their relative strengths are tabulated in Table 1. The results indicate pulsewidth-dependent broadening

of the reconstructed beamlets. For the treatment and detection settings considered in this simulation, we observed that each beamlet cannot be resolved for proton beam pulsewidths $\geq 4\mu$s. For larger pulse durations as well as smaller separation between beamlets, a larger transducer array aperture and smaller pitch would be beneficial. This issue can also be ameliorated via deconvolving the pulse function from the collected signals as well as by employing advanced reconstruction algorithms, which incorporate finite pulsewidths in the model. This will be the focus of our future research.
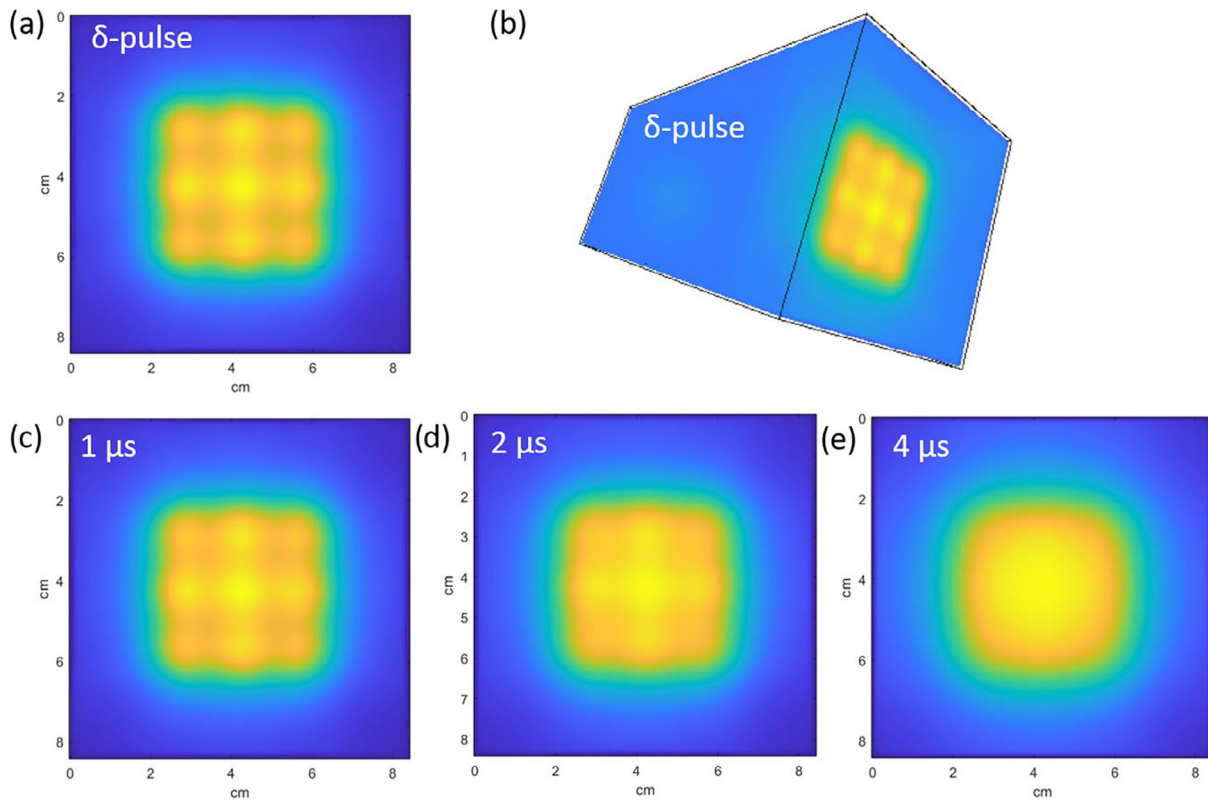
FIGURE 6 (a) XY slice taken from the 3D TR δ-pulse reconstruction of the multi-beam proton deposition file at the center of the Bragg peak. (b) 3D volumetric view of the reconstructed δ-pulse 9 beam file. Reconstructed XY slice at the Bragg peak for (c) 1 μs, (d) 2 μs, and (e) 4 μs pulse durations.

TABLE 1 FWHM and relative intensity values for each beam spot in Figures 5(b) and 6(a).

Spot number	Ground truth FWHM$_H$ (cm)	Reconstructed FWHM$_H$ (cm)			Ground truth FWHM$_V$ (cm)	Reconstructed FWHM$_V$ (cm)			Relative intensities		
		δ-pulse	1 μs PW	2 μs PW		δ-pulse	1 μs PW	2 μs PW	δ-pulse	1 μs PW	2 μs PW
1	1.14	1.65	1.75	1.78	1.11	1.64	1.72	1.76	0.83	0.86	0.88
2	1.10	1.38	1.41	1.80	1.09	1.63	1.73	1.78	0.95	0.94	0.95
3	1.19	1.71	1.78	1.84	1.13	1.67	1.75	1.77	0.83	0.85	0.86
4	1.14	1.68	1.77	1.81	1.16	1.44	1.45	1.78	0.95	0.94	0.95
5	1.11	1.39	1.41	1.74	1.16	1.39	1.42	1.77	1	1	1
6	1.14	1.71	1.79	1.86	1.13	1.42	1.44	1.80	0.95	0.92	0.93
7	1.09	1.64	1.76	1.79	1.13	1.67	1.76	1.86	0.83	0.85	0.86
8	1.19	1.42	1.42	1.77	1.11	1.71	1.78	1.84	0.95	0.92	0.93
9	1.08	1.73	1.80	1.87	1.13	1.72	1.78	1.85	0.83	0.83	0.85

4 | DISCUSSION

The purpose of this simulation study is to provide characteristics and feasibility behind protoacoustics as a dosimeter for FLASH proton therapy. To demonstrate that protoacoustics can be applied to FLASH, dose rates were varied between 5 and 20 cGy/pulse through simulation, where linearity was achieved with no saturation despite increased dose per pulses. Pulsewidths were varied to show the effects on the protoacoustic signal. The simulations also introduce the use of a linear array, which would allow for higher imaging speed and 3D reconstruction.

For protoacoustics, one of the key characteristics that make this a strong dosimeter is the linearity that is observed between the dose and pressure signal as

well as real time monitoring. From Figure 4(b), a linear response can be seen, even with dose per pulses that are nearly a 100 times greater than the dose per pulse achieved by current clinical machines (0.2 vs. 20 cGy/pulse). Although it's known that this linear trend is observed throughout most dosimeters, this has mostly been with conventional therapy doses and not ultra-high dose rates, which is what is shown through this simulation.[51] Most dosimeters, such as the ion chamber, have difficulties in these high dose rate ranges with saturation. However, we have demonstrated a constant linear trend despite these dose rates being a barrier for many other dosimeters. Although this simulation work only covers between 0.2 and 20 cGy/pulse for varied doses, it's possible that the detected dose can be even lower or higher and can be tested in future works. Based on several other works that have been completed, the dynamic range for protoacoustics has been shown to be very large. In the paper by Hickling et al., a dose as low as 11.6 mGy was detected using XACT.[52] Linearity for even higher dose per pulses have not been explored within this work, but machines, such as the Mevion synchrocyclotron demonstrate FLASH capabilities using 16–32 cGy/pulse. Within this range, the pressure from the FLASH proton energy will not be strong enough to cause non-linear effects.[39] With FLASH radiotherapy (FLASH-RT), pressure levels can reach significantly higher levels compared to conventional radiotherapy, which is only on the order of mPa.[21,53] With current levels of pressure seen in FLASH, commercially available transducers can detect signals without any concerns for nonlinearity.[34] In fact, because of such a high acoustic signal, significant amplification or signal averaging is necessary due to higher dose rates yielding increased SNR.

Using the dose rates in the simulation, the pulse repetition rate would need to be higher compared to what is typically observed in electron-based FLASH-capable machines. The Mevion synchrocyclotron reaches FLASH conditions through a pulse repetition rate of 648 Hz and dose rate between 16 and 32 cGy/pulse, which is significantly higher than the pulse repetition rates seen in electron-based FLASH machines, which were reported around 100−200 Hz.[39] Based on the Mevion proton machine, which is capable of a pulse repetition rate of 750 Hz, a dose rate of as low as 5.33 cGy/pulse is possible for FLASH (40 Gy/s).

The acoustic pressure signal from the k-Wave simulations were convoluted with a Gaussian pulse to vary the pulsewidth. Studying the pulsewidth of the signal is crucial as the effects of the signal generation efficiency based on this parameter must still be characterized. Several different proton machines are capable of FLASH with various pulsewidths. Within clinical machines, many vary in the microsecond range.[39,54,55] When encompassing non-clinical machines, there has already been development of laser-driven proton sources with pulsewidths in the nanosecond range. The Mevion synchrocyclotron uses pulsewidths between 4 and 6 μs conventionally, while demonstrating FLASH with 20 μs pulsewidths. Although it is not expected that protoacoustics could be used for isochronus cyclotrons with quasi-continuous beams, it's been demonstrated that the generated pulses could be segmented into 18 μs pulsewidths.[21]

To further demonstrate this concept, pulsewidths between 0.1 and 20 μs were used in Figure 4(a) to observe the characteristics of the protoacoustic signal due to changes in pulse duration. With decreasing pulse duration, an increase in the acoustic pressure signal is viewed. This trend is better seen in Figure 4(b), where the maximum pressure signal amplitude for each pulsewidth is plotted and fitted to an exponential curve. For pulsewidths between 0.1 and 1 μs, the pressure amplitude has been demonstrated to plateau as it satisfies stress confinement.[38] Therefore, the data points in Figure 4(b) are fitted to the pulsewidths larger than 1 μs. Similar reconstruction results with the increasing beam size with increasing pulsewidths can also be viewed in Sanbul et al.'s paper, where 2D reconstructions were performed on electron-based FLASH.[34] The broadening effect is based on the increase in the pulsewidth, which could potentially lead to loss in quantitative dose. Future work incorporating temporally broader beam profiles in the reconstruction schemes will be completed to explore this characteristic further.

Reconstruction of small proton beam spots is demonstrated in this work. The paper by Prezado and Fois uses a beam spot size of 3 mm, which is what we include in our paper.[56] In minibeam radiation therapy, the beam sizes go down to 0.7 mm, which is why we explore smaller beams in the simulation. LATTICE radiation therapy (LRT) also falls under SFRT, and has been used in over 150 patients. To demonstrate the potential protoacoustics has over other dosimeters, a 3D reconstruction was performed using a proton beam profile with 9 beams, similar to LRT[37] (Figure 3). LRT is an upcoming approach for radiation therapy that uses an array of high dose regions. The capability of protoacoustics to facilitate 3D proton dose reconstruction is significant for several reasons. Many dosimeters are unable to perform 3D reconstructions because it would require the use of a matrix array or the system is only capable of point measurements. These systems are also not typically in vivo nor real-time, which are the key characteristics of protoacoustics. Although protoacoustics displays such strengths, there are slight setbacks with the resolution. The reconstruction shown in this study was completed using an 8 cm × 8 cm detector, where each individual beam was distinguishable with beam size not varying between each one. A 5 cm × 5 cm detector size was initially for the planar array in the simulation. However, using this detector, an image could not properly be resolved. This is due to the detector not being

large enough for the 9 beam profile. Table 1 displays the FWHM (4) for each beam spot from Figure 6, with beams being listed left to right. The profiles along the horizontal and vertical lines as shown in Figure 5(b) were fitted to gaussians. FWHMs are also obtained from the fitting and are tabulated in Table 1 along with the true values, which are extracted from the simulated TOPAS energy deposition map. Beam 5 has the best and uniform angular coverage of the detector grid, hence why its FWHM is expected to be the smallest and similar along the horizontal and vertical. Beams 1,3,7, and 9 are expected to have the largest FWHM. Moreover, as expected from the symmetry of the problem, the horizontal (and vertical) FWHMs of beams 2 and 8 are similar to the vertical (and horizontal) FWHMs of beams 4 and 6.

5 | CONCLUSION

Through this simulation study, the possibility of using protoacoustics in proton FLASH therapy was explored and verified through the variation of different parameters to match FLASH characteristics. Clinical energy proton beam was used in the study and the dose per pulse was varied between conventional and FLASH parameters. From this, we were able to verify the wide dynamic range for protoacoustics while maintaining the linearity between the dose and measured acoustic pressure. The pulsewidth was also varied through simulation and 2D reconstructions were performed to see the effects the parameter has on signal generation and the proton beam itself. With the reconstructions, an increase in the diameter of the beam was observed with increasing pulsewidth. 3D reconstruction was also possible using an 8 cm × 8 cm planar array, with high visibility of each beam. The results of this simulation work shows the potential of protoacoustics being implemented in clinics for its linearity even with FLASH parameters. Future works for simulations include further variation of the dose per pulse to show the full dynamic range of protoacoustics. We also aim to develop advanced model-based reconstruction algorithms to correct the pulsewidth-induced broadening of the reconstructed beam profiles. Tissue heterogeneity is another parameter that will also be explored in the protoacoustic reconstructions by using information obtained from a complimentary imaging method such as ultrasound, CT or MRI. Further studies should also look into the potential cavitation effects that occur with much higher dose per pulses and shorter proton pulses.

CONFLICT OF INTEREST STATEMENT
The authors have no conflicts to disclose.

REFERENCES
1. Siegel RL, Miller KD, Fuchs HE, Jemal A. Cancer statistics, 2022. *CA Cancer J Clin*. 2022;72(1):7-33. doi:10.3322/CAAC.21708
2. Gianfaldoni S, Gianfaldoni R, Wollina U, Lotti J, Tchernev G, Lotti T. An overview on radiotherapy: from its history to its current applications in dermatology. *Open Access Maced J Med Sci*. 2017;5(4):521. doi:10.3889/OAMJMS.2017.122
3. Yang M, Wang X, Guan F, et al. Physics and biology of ultrahigh dose-rate (FLASH) radiotherapy: a topical review. *Phys Med Biol*. 2020;65(23):23TR03. doi:10.1088/1361-6560/ABAA28
4. Favaudon V, Caplier L, Monceau V, et al. Ultrahigh dose-rate FLASH irradiation increases the differential response between normal and tumor tissue in mice. *Sci Transl Med*. 2014;6(245):245ra93. doi:10.1126/SCITRANSLMED.3008973
5. Romano F, Bailat C, Jorge PG, Lerch MLF, Darafsheh A. Ultra-high dose rate dosimetry: challenges and opportunities for FLASH radiation therapy. *Med Phys*. 2022;49(7):4912-4932. doi:10.1002/MP15649
6. Kim MM, Darafsheh A, Schuemann J, et al. Development of ultra-high dose-rate (FLASH) particle therapy. *IEEE Trans Radiat Plasma Med Sci*. 2022;6(3):252-262. doi:10.1109/TRPMS.2021.3091406
7. Diffenderfer ES, Sørensen BS, Mazal A, Carlson DJ. The current status of preclinical proton FLASH radiation and future directions. *Med Phys*. 2022;49(3):2039-2054. doi:10.1002/MP15276
8. Singers Sørensen B, Krzysztof Sitarz M, Ankjærgaard C, et al. In vivo validation and tissue sparing factor for acute damage of pencil beam scanning proton FLASH. *Radiother Oncol*. 2022;167:109-115. doi:10.1016/J.RADONC.2021.12.022
9. Vozenin MC, Hendry JH, Limoli CL. Biological benefits of ultra-high dose rate FLASH radiotherapy: sleeping beauty awoken. *Clin Oncol (R Coll Radiol)*. 2019;31(7):407-415. doi:10.1016/J.CLON.2019.04.001
10. Montay-Gruel P, Petersson K, Jaccard M, et al. Irradiation in a flash: unique sparing of memory in mice after whole brain irradiation with dose rates above 100 Gy/s. *Radiother Oncol*. 2017;124(3):365-369. doi:10.1016/J.RADONC.2017.05.003
11. Bourhis J, Montay-Gruel P, Gonçalves Jorge P, et al. Clinical translation of FLASH radiotherapy: why and how? *Radiother Oncol*. 2019;139:11-17. doi:10.1016/J.RADONC.2019.04.008
12. Jolly S, Owen H, Schippers M, Welsch C. Technical challenges for FLASH proton therapy. *Phys Med*. 2020;78:71-82. doi:10.1016/J.EJMP.2020.08.005
13. Ashraf MR, Rahman M, Zhang R, et al. Dosimetry for FLASH radiotherapy: a review of tools and the role of radioluminescence and cherenkov emission. *Front Phys*. 2020;8:328. doi:10.3389/FPHY.2020.00328/BIBTEX
14. McManus M, Romano F, Lee ND, et al. The challenge of ionisation chamber dosimetry in ultra-short pulsed high dose-rate Very High Energy Electron beams. *Sci Rep*. 2020;10(1):9089. doi:10.1038/S41598-020-65819-Y
15. Romano F, Subiel A, McManus M, et al. Challenges in dosimetry of particle beams with ultra-high pulse dose rates. *J Phys Conf Ser*. 2020;1662(1):012028. doi:10.1088/1742-6596/1662/1/012028

16. Kranzer R, Schüller A, Bourgouin A, et al. Response of diamond detectors in ultra-high dose-per-pulse electron beams for dosimetry at FLASH radiotherapy. *Phys Med Biol*. 2022;67(7):075002. doi:10.1088/1361-6560/AC594E

17. Verona Rinati G, Felici G, Galante F, et al. Application of a novel diamond detector for commissioning of FLASH radiotherapy electron beams. *Med Phys*. 2022;49(8):5513-5522. doi:10.1002/MP.15782

18. Jorge PG, Jaccard M, Petersson K, et al. Dosimetric and preparation procedures for irradiating biological models with pulsed electron beam at ultra-high dose-rate. *Radiother Oncol*. 2019;139:34-39. doi:10.1016/J.RADONC.2019.05.004

19. Anton M. Uncertainties in alanine/ESR dosimetry at the Physikalisch-Technische Bundesanstalt. *Phys Med Biol*. 2006;51(21):5419. doi:10.1088/0031-9155/51/21/003

20. Akselrod MS, Sykora GJ. Fluorescent nuclear track detector technology—a new way to do passive solid state dosimetry. *Radiat Meas*. 2011;46(12):1671-1679. doi:10.1016/J.RADMEAS.2011.06.018

21. Jones KC, Vander Stappen F, Bawiec CR, et al. Experimental observation of acoustic emissions generated by a pulsed proton beam from a hospital-based clinical cyclotron. *Med Phys*. 2015;42(12):7090-7097. doi:10.1118/1.4935865

22. Sulak L, Armstrong T, Baranger H, et al. Experimental studies of the acoustic signature of proton beams traversing fluid media. *Nucl Instrum Methods*. 1979;161(2):203-217. doi:10.1016/0029-554X(79)90386-0

23. Tada J, Hayakawa Y, Hosono K, Inada T. Time resolved properties of acoustic pulses generated in water and in soft tissue by pulsed proton beam irradiation—a possibility of doses distribution monitoring in proton radiation therapy. *Med Phys*. 1991;18(6):1100-1104. doi:10.1118/1.596618

24. Nie W, Jones KC, Petro S, Kassaee A, Sehgal CM, Avery S. Proton range verification in homogeneous materials through acoustic measurements. *Phys Med Biol*. 2018;63(2):025036. doi:10.1088/1361-6560/AA9C1F

25. Samant P, Trevisi LM, Chen Y, Zwart T, Xiang L. 3D protoacoustic imaging through a planar ultrasound array: a simulation workflow. *IEEE Trans Radiat Plasma Med Sci*. 2022;7(1):83-95. doi:10.1109/TRPMS.2022.3177236. Published online May 26.

26. Durante M, Paganetti H, Knopf AC, Lomax A. In vivo proton range verification: a review. *Phys Med Biol*. 2013;58(15):R131. doi:10.1088/0031-9155/58/15/R131

27. Assmann W, Kellnberger S, Reinhardt S, et al. Ionoacoustic characterization of the proton Bragg peak with submillimeter accuracy. *Med Phys*. 2015;42(2):567-574. doi:10.1118/1.4905047

28. Lehrack S, Assmann W, Bertrand D, et al. Submillimeter ionoacoustic range determination for protons in water at a clinical synchrocyclotron. *Phys Med Biol*. 2017;62(17):L20. doi:10.1088/1361-6560/AA81F8

29. Patch SK, Santiago-Gonzalez D, Mustapha B. Thermoacoustic range verification in the presence of acoustic heterogeneity and soundspeed errors—Robustness relative to ultrasound image of underlying anatomy. *Med Phys*. 2019;46(1):318-327. doi:10.1002/MP13256

30. Van Dongen KWA, De Blécourt AJ, Lens E, Schaart DR, Vos FM. Reconstructing 3D proton dose distribution using ionoacoustics. *Phys Med Biol*. 2019;64(22):225005. doi:10.1088/1361-6560/AB4CD5

31. Ahmad M, Xiang L, Yousefi S, Xing L. Theoretical detection threshold of the proton-acoustic range verification technique. *Med Phys*. 2015;42(10):5735. doi:10.1118/1.4929939

32. Kellnberger S, Assmann W, Lehrack S, et al. Ionoacoustic tomography of the proton Bragg peak in combination with ultrasound and optoacoustic imaging. *Sci Rep*. 2016;6(1):1-7. doi:10.1038/srep29305

33. Patch SK, Nguyen C, Dominguez-Ramirez D, et al. Thermoacoustic range verification during pencil beam delivery of a clinical plan to an abdominal imaging phantom. *Radiother Oncol*. 2021;159:224-230. doi:10.1016/J.RADONC.2021.03.027

34. Ba Sunbul NH, Zhang W, Oraiqat I, et al. A simulation study of ionizing radiation acoustic imaging (iRAI) as a real-time dosimetric technique for ultra-high dose rate radiotherapy (UHDR-RT). *Med Phys*. 2021;48(10):6137-6151. doi:10.1002/MP.15188

35. Oraiqat I, Zhang W, Litzenberg D, et al. An ionizing radiation acoustic imaging (iRAI) technique for real-time dosimetric measurements for FLASH radiotherapy. *Med Phys*. 2020;47(10):5090-5101. doi:10.1002/MP.14358

36. Yan W, Khan MK, Wu X, et al. Spatially fractionated radiation therapy: history, present and the future. *Clin Transl Radiat Oncol*. 2020;20:30-38. doi:10.1016/j.ctro.2019.10.004

37. Wu X, Perez NC, Zheng Y, et al. The technical and clinical implementation of LATTICE Radiation Therapy (LRT). *Radiat Res*. 2020;194(6):737-746. doi:10.1667/RADE-20-00066.1

38. Jones KC, Seghal CM, Avery S. How proton pulse characteristics influence protoacoustic determination of proton-beam range: simulation studies. *Phys Med Biol*. 2016;61(6):2213. doi:10.1088/0031-9155/61/6/2213

39. Darafsheh A, Hao Y, Zwart T, et al. Feasibility of proton FLASH irradiation using a synchrocyclotron for preclinical studies. *Med Phys*. 2020;47(9):4348-4355. doi:10.1002/MP.14253

40. Felici G, Barca P, Barone S, et al. Transforming an IORT Linac into a FLASH research machine: procedure and dosimetric characterization. *Front Phys*. 2020;8:374. doi:10.3389/FPHY.2020.00374/BIBTEX

41. Xu M, Wang LV. Photoacoustic imaging in biomedicine. *Rev Sci Instrum*. 2006;77(4):041101. doi:10.1063/1.2195024

42. Hickling S, Xiang L, Jones KC, et al. Ionizing radiation-induced acoustics for radiotherapy and diagnostic radiology applications. *Med Phys*. 2018;45(7):e707-e721. doi:10.1002/MP.12929

43. Treeby BE, Cox BT. k-Wave: mATLAB toolbox for the simulation and reconstruction of photoacoustic wave fields. *J Biomed Opt*. 2010;15(2):021314. doi:10.1117/1.3360308

44. Hepler LG. Thermal expansion and structure in water and aqueous solutions. *Canad J Chem*. 1969;47(24):4613-4617. doi:10.1139/V69-762

45. Petrova E, Ermilov S, Su R, Nadvoretskiy V, Conjusteau A, Oraevsky A. Using optoacoustic imaging for measuring the temperature dependence of Grüneisen parameter in optically absorbing solutions. *Opt Express*. 2013;21(21):25077. doi:10.1364/OE.21.025077

46. Faddegon B, Ramos-Méndez J, Schuemann J, et al. The TOPAS tool for particle simulation, a Monte Carlo simulation tool for physics, biology and clinical research. *Phys Med*. 2020;72:114-121. doi:10.1016/J.EJMP.2020.03.019

47. Wei C, Jing T, Ji Y, et al. Improvements in the stopping power library libdEdx and release of the web GUI dedx.au.dk. *J Phys Conf Ser*. 2014;489(1):012003. doi:10.1088/1742-6596/489/1/012003

48. Xia J, Yao J, Wang LV. Photoacoustic tomography: principles and advances. *Electromagn Waves (Camb)*. 2014;147:1-22. doi:10.2528/PIER14032303

49. Hughes JR, Parsons JL. FLASH radiotherapy: current knowledge and future insights using proton-beam therapy. *Int J Mol Sci*. 2020;21(18):1-14. doi:10.3390/IJMS21186492

50. Jiang Z, Sun L, Yao W, Wu QJ, Xiang L, Ren L. 3D in vivo dose verification in prostate proton therapy with deep learning-based proton-acoustic imaging. *Phys Med Biol*. 2022;67(21):215012. doi:10.1088/1361-6560/AC9881

51. Scampoli P, Carpentieri C, Giannelli M, et al. Radiobiological characterization of the very high dose rate and dose per pulse electron beams produced by an IORT (intra operative radiation therapy) dedicated linac. *Transl Cancer Res*. 2017;6(S5):S761-S768. https://doi.org10.21037/TCR.2017.05.21

52. Hickling S, Hobson M, El Naqa I. Characterization of x-ray acoustic computed tomography for applications in radiotherapy

dosimetry. *IEEE Trans Radiat Plasma Med Sci*. 2018;2(4):337-344. doi:10.1109/TRPMS.2018.2801724

53. Lascaud J, Parodi K. On the potential biological impact of radiation-induced acoustic emissions during ultra-high dose rate electron radiotherapy: a preliminary study. *Phys Med Biol*. 2023;68(5):05LT01. doi:10.1088/1361-6560/ACB9CE

54. Akulinichev SV, Vasiliev VN, Gavrilov YK, et al. Possibilities of proton FLASH therapy on the accelerator at the Russian Academy of Sciences' Institute for Nuclear Research. *Bull Russ Acad Sci: Phys*. 2020;84(11):1325-1329. doi:10.3103/S1062873820110039/FIGURES/2

55. Bin J, Allinger K, Assmann W, et al. A laser-driven nanosecond proton source for radiobiological studies. *Appl Phys Lett*. 2012;101(24):243701. doi:10.1063/1.4769372

56. Prezado Y, Fois GR. Proton-minibeam radiation therapy: a proof of concept. *Med Phys*. 2013;40(3):031712. doi:10.1118/1.4791648

How to cite this article: Kim K, Pandey PK, Gonzalez G, Chen Y, Xiang L. Simulation study of protoacoustics as a real-time in-line dosimetry tool for FLASH proton therapy. *Med. Phys*. 2023;:1-11. https://doi.org/10.1002/mp.16894